nesian villages and towns, and there is now grave concern that recent stress changes to their north and west will have moved each zone closer to rupture. The Nias earthquake on 28 March 2005 confirms that stress changes from the 26 December earthquake, though small (*6*), were sufficient to push this contiguous 300-km segment of plate boundary to the point of failure. The 3-month delay between the two earthquakes has awakened fears that a domino-like failure of the already highly stressed plate boundary to the south and east may follow.

Nobody familiar with the history or geology of the Sumatra/Andaman arc could have foreseen the magnitude of the 26 December 2004 earthquake, nor is there a precedent for its complexity (Fig. 1). The rupture initiated at 3.3°N near a blunt corner of the arc, where the almost-passive junction between the Indian and Australian plates plunges northeastward beneath the islands. Ammon *et al*. (*7*) report the analysis of *P* waves (the first-arriving and fastest waves that travel outward from an earthquake) digitally recorded by seismometers around the world. Their analysis reveals that during its first minute, the earthquake broke a 100-km patch of the plate boundary rather slowly northward. Had it stopped there, its magnitude would have perhaps reached a high 7, typical of historical events to the north. But instead of slowing, the rupture accelerated to 3 km/s for the next 4 min and thereafter maintained an average speed of about 2.5 km/s for a further 6 min.

The rupture front that marked the fracture of the Nicobar/Andaman plate boundary propagated like a noisy fire engine traveling to the northwest. Seismometers in Russia listening to its approach heard the sound at a higher pitch than did similar seismometers in Australia, which sensed the fracture receding from them [Lay *et al*. (*8*)]. In this sense, seismometers in Australia observed the rupture at longer wavelengths, just like the redshift of a receding galaxy caused by the Doppler effect in light waves. Ammon *et al*. note that the Doppler shift was not uniform in time. They attribute the changes in amplitude and wobbles in the Doppler shift to occasional acceleration and deceleration, or hesitation, of the rupture during its passage northward.

But the most remarkable feature of the earthquake was not the 8050-km/hour, 10-min urgency that characterizes the initial unzipping of the plate boundary; it was its slow subsequent slip. Slip occurred at typical rupture speeds in the south, sufficiently fast to propel the tsunami on its destructive worldwide journey. However, at its northern end, the surface between the Indian plate and the Andaman archipelago took more than half an hour to slide a distance of 7 to 20 m. It was this slow slip that tripled the quake's energy release from *M* 9 to a gigantic *M* 9.3. Slip occurred too slowly in the last 5 min to generate either tsunamis or sizable 20-s surface waves (the amplitudes of which are used to assign a Richter magnitude for an earthquake). After adjusting their computer codes, seismologists quantified this slow slip from the amplitude of waves with 20-min periods and longer, which circumnavigated the globe each hour for several days. Park *et al*. indicate that the longest-period waves were visible for weeks (*9*).

The slowness of this slip excited several of Earth's fundamental resonances. From these relative amplitudes, Park *et al*. surmise that the northern end of the rupture released one-third of the total energy in the earthquake, equivalent to an M_w 8.9 (*9*). This slow slip moved Global Positioning System (GPS) points on the Andaman Islands by more than 4 m toward southern India (*10*), sinking some shores and raising others. Tide gauge data recorded no subsidence for 30 min after seismic shaking, confirming the delayed timing of this slip (*3*, *11*).

It is sobering to realize that if this northern slip had not been slow, it would have generated tsunamigenic waves along the entire 1300-km-long rupture zone, causing more widespread and more severe damage on the coastlines of India, Myanmar, and Thailand. This aside, many seismologists are now wondering whether their past assessments of future seismic hazard elsewhere have been too conservative. Seismic hazards on numerous plate boundaries, such as the nearby Himalaya, have been assessed until now in terms of recent history, without the benefit of an extended record that may contain extreme events (*12*). The 2004 Sumatra-Andaman earthquake is a wake-up call that conservative seismic forecasts may not serve society well.

References and Notes

1. M. West, J. J. Sánchez, S. R. McNutt, *Science* **308**, 1144 (2005).
2. M. Ortiz, R. Bilham, *J. Geophys. Res.* **108**, 1029/2002JB001941 (2003).
3. R. Bilham, E. R. Engdahl, N. Feldl, S. P. Satyabala, *Seism. Res. Lett.*, in press.
4. P. Cummins, M. Leonard, *AusGeo News* No. 77 (March 2005).
5. These posters were distributed in field seasons before the 2004 earthquake (see www.tectonics.caltech.edu/sumatra/downloads/20040604SumatraPoster.ppt).
6. J. McCloskey, S. Nalbant, S. Steacy, K. Sieh, *Nature*, in press.
7. C. J. Ammon *et al.*, *Science* **308**, 1133 (2005).
8. T. Lay *et al.*, *Science* **308**, 1127 (2005).
9. J. Park *et al.*, *Science* **308**, 1139 (2005).
10. S. Jade, V. K. Gaur, M. B. Ananda, P. D. Kumar, S. Banerjee, *Current Sci.*, in press.
11. C. P. Rajendran, A. Earnest, K. Rajendran, R. Bilham, J. Freymueller, in preparation.
12. R. Bilham, K. Wallace, *Geol. Surv. India Spec. Pub.* **85**, 1 (2005).
13. J. Curry, *J. Asian Earth Sci.* **25**, 187 (2005).
14. M. Ishii, P. M. Shearer, H. Houston, J. E. Vidale, *Nature*, in press.
15. P. Banerjee, F. F. Pollitz, R. Bürgmann, *Science* 19 May 2005 (10.1126/science.1113746).

10.1126/science.1113363

RESEARCH ARTICLE

The Great Sumatra-Andaman Earthquake of 26 December 2004

Thorne Lay,[1,2]* Hiroo Kanamori,[3] Charles J. Ammon,[4] Meredith Nettles,[5] Steven N. Ward,[2] Richard C. Aster,[6] Susan L. Beck,[7] Susan L. Bilek,[6] Michael R. Brudzinski,[8,9] Rhett Butler,[10] Heather R. DeShon,[8] Göran Ekström,[5] Kenji Satake,[11] Stuart Sipkin[12]

The two largest earthquakes of the past 40 years ruptured a 1600-kilometer-long portion of the fault boundary between the Indo-Australian and southeastern Eurasian plates on 26 December 2004 [seismic moment magnitude (M_w) = 9.1 to 9.3] and 28 March 2005 (M_w = 8.6). The first event generated a tsunami that caused more than 283,000 deaths. Fault slip of up to 15 meters occurred near Banda Aceh, Sumatra, but to the north, along the Nicobar and Andaman Islands, rapid slip was much smaller. Tsunami and geodetic observations indicate that additional slow slip occurred in the north over a time scale of 50 minutes or longer.

The 26 December 2004 Sumatra-Andaman earthquake was the largest seismic event on Earth in more than 40 years, and it produced the most devastating tsunami in recorded history (*1*). Like other comparably sized great earthquakes—such as the 1952 Kamchatka, the 1957 Andreanof Islands in the Aleutians, the 1960 Southern Chile, and the 1964 Prince William Sound, Alaska, earthquakes—the Sumatra-Andaman event ruptured a subduction zone megathrust plate boundary. These giant earthquakes occur where large oceanic plates underthrust continental margins. They involve huge fault areas, typically 200 km wide by 1000 km long, and large fault slips of 10 m or more. Such events dwarf the contributions to plate motion of vast numbers of lower magnitude earthquakes. The high tsunami-

associated death toll appears to have been due to the dense population of the affected region. The tsunami magnitude, M_t, of the earthquake was 9.1 (*2*), as compared to M_t = 9.1 for the 1964 Alaska and M_t = 9.4 for the 1960 Chile earthquakes (*3*). The event ruptured 1200 to 1300 km of a curved plate boundary, with variations in direction of interplate motion and age of subducting lithosphere apparently affecting the nature of the faulting. The 28 March 2005 event ruptured an adjacent 300-km-long portion of the plate boundary (*4*). These two events are the largest to occur after the global deployment of digital broadband, high-dynamic-range seismometers (*5*, *6*), which recorded both the huge ground motions from the mainshocks and the tiny motions from ensuing free oscillations of the planet and from small aftershocks (*7*, *8*). In this and two companion papers (*9*, *10*), we report on the nature of faulting in these great earthquakes based on seismological analyses of the extensive, openly available seismogram data set from the international Federation of Digital Seismic Networks (FDSN) backbone network (*5*, *6*).

Plate geometry and setting. The 2004 and 2005 earthquakes ruptured the boundary between the Indo-Australian plate, which moves generally northward at 40 to 50 mm/year, and the southeastern portion of the Eurasian plate, which is segmented into the Burma and Sunda subplates (Fig. 1). East of the Himalayas, the plate boundary trends southward through Myanmar, continuing offshore as a subduction zone along the Andaman and Nicobar Islands south to Sumatra, where it turns eastward along the Java trench (*11*). As a result of the highly oblique motion between the Indo-Australian plate and the Burma and Sunda subplates (Fig. 1), a plate sliver, referred to as the Andaman or Burma microplate, has sheared off parallel to the subduction zone from Myanmar to Sumatra (*12*). Oblique, but predominantly thrust, motion occurs in the Andaman trench with a convergence rate of about 14 mm/year (*13*, *14*). The Andaman Sea ridge-transform system, an oblique back-arc spreading center, accommodates the remaining plate motion, joining with the Sumatra Fault to the south (*15*, *16*). Underthrusting along the Sunda trench, with some right-lateral faulting on the inland Sumatra Fault, accommodates interplate motion along Sumatra.

Historic great earthquakes along this plate boundary occurred in 1797 [magnitude (M) ~ 8.4], 1833 (M ~ 9), and 1861 (M ~ 8.5) (*17*, *18*), providing the basis for the long-recognized potential for great earthquakes along Sumatra (*11*, *19*). A smaller (M ~ 7.8) event in 1907 just south of the 2004 rupture zone produced seismic and tsunami damage in northern Sumatra (*11*). These events all occurred to the southeast of the 2004 rupture zone (Fig. 1). The 28 March 2005 event ruptured the same region as the 1861 and 1907 events (Fig. 1). Smaller events in the Andaman trench, also presumed to involve thrusting motions, occurred beneath the Nicobar Islands in 1881 (M ~ 7.9) and near the Andaman Islands in 1941 (M ~ 7.9). There is no historical record of a previous tsunamigenic earthquake in the Bay of Bengal comparable to the 2004 event (*12*).

In the 40 years preceding the 2004 event, little seismicity occurred within 100 km of the trench in the region between the 2004 and 1881 epicenters (figs. S1 to S3). Similarly, seismicity was low in the source region of the great 1861 earthquake before the 28 March 2005 event and is still low in the 1833 rupture region (fig. S2). Numerous earthquakes occurred near the 2004 epicenter in recent years, including a seismic-moment magnitude (M_w) = 7.2 event in 2002. These features are consistent with long-term strain accumulation in the eventual rupture zone and stress concentration in the vicinity of the mainshock hypocenter.

The mainshocks. The 2004 mainshock rupture began at 3.3°N, 96.0°E, at a depth of about 30 km, at 00:58:53 GMT (*1*). The Harvard centroid-moment-tensor (CMT) solution indicates predominantly thrust faulting on a shallowly (8°) dipping plane with a strike of 329° (*20*, *21*). The rake (110°) indicates a slip direction ~20° closer to the trench-normal direction than to the interplate convergence direction, consistent with some long-term par-

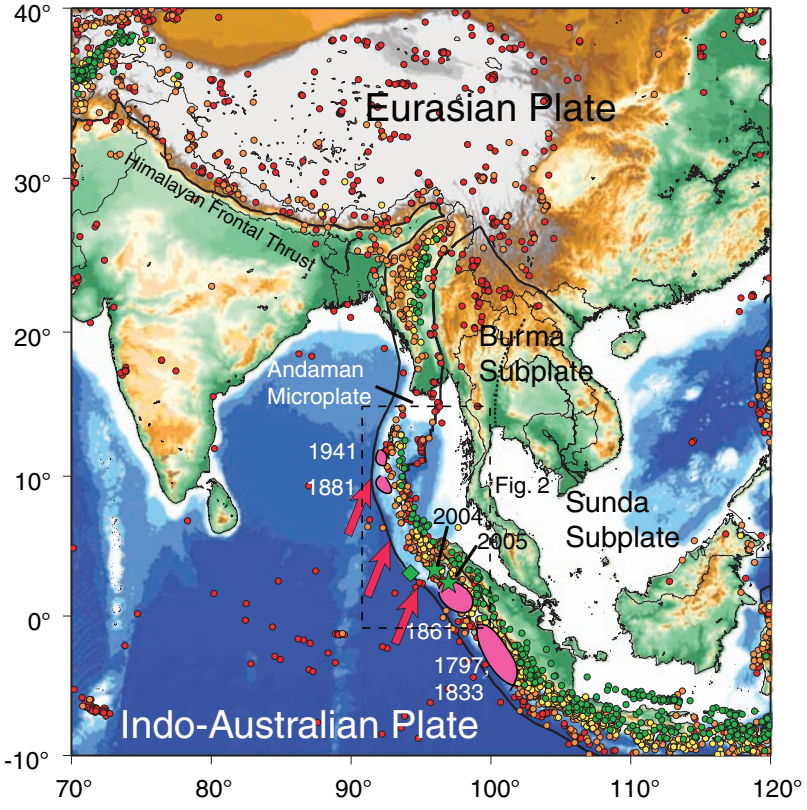

Fig. 1. Regional map showing earthquakes with magnitudes >5.0 from 1965 to 25 December 2004 from the earthquake catalog of the National Earthquake Information Center (NEIC). Red dots show events with depths <33 km; orange, depths of 33 to 70 km; yellow, depths of 70 to 105 km; and green, depths >105 km. Locations of previous large earthquake ruptures along the Sunda-Andaman trench system are shown in pink. Dashed box shows area of the map in Fig. 2. Green stars show the epicenters of the two recent great events; the green diamond shows the CMT centroid location for the 2004 Sumatra-Andaman event. The thick red arrows indicate the NUVEL-1 relative plate motions between the Indo-Australian and Eurasian plates.

[1]Earth Sciences Department and [2]Institute of Geophysics and Planetary Physics, University of California, Santa Cruz, CA 95064, USA. [3]Seismological Laboratory, California Institute of Technology, MS 252-21, Pasadena, CA 91125, USA. [4]Department of Geosciences, The Pennsylvania State University, 440 Deike Building, University Park, PA 16802, USA. [5]Department of Earth and Planetary Sciences, Harvard University, 20 Oxford Street, Cambridge, MA 02138, USA. [6]Department of Earth and Environmental Science and Geophysical Research Center, New Mexico Institute of Mining and Technology, Socorro, NM 87801, USA. [7]Department of Geosciences, The University of Arizona, Gould-Simpson Building #77, Tucson, AZ 85721, USA. [8]Department of Geology and Geophysics, University of Wisconsin–Madison, 1215 West Dayton St., Madison, WI 53706, USA. [9]Geology Department, Miami University, Oxford, OH 45056, USA. [10]IRIS Consortium, 1200 New York Avenue, NW, Washington, DC, 20005, USA. [11]Geological Survey of Japan, Advanced Industrial Sciences and Technology, Site C7 1-1-1 Higashi, Tsukuba 305-8567, Japan. [12]National Earthquake Information Center, U.S. Geological Survey, Golden, CO 80401, USA.

*To whom correspondence should be addressed. E-mail: thorne@pmc.ucsc.edu

titioning of right-lateral motion onto the Sumatra Fault, which is not reported to have ruptured during the 2004 event. The aftershock distribution (Fig. 2) gives a first-order indication of the extent of the mainshock ruptures. For the 2004 event, the distribution suggests a rupture length of 1300 km extending from northwestern Sumatra to the Andaman Islands. Along the northern extension of the aftershock zone, the strike of the fault rotates progressively clockwise (Fig. 2). The associated degree of right-lateral slip (rake >90°) on the megathrust fault should increase to the north unless that component of interplate motion is partitioned onto the back-arc transform system. Given the variation in the relative plate motion along the aftershock zone, it is surprising that the CMT solution is a nearly pure double-couple source, indicative of simple faulting geometry. The faulting solution favors a concentration of <500 s period seismic radiation in the southern portion of the aftershock zone, as does the location of the centroid, which lies about 160 km west of the epicenter (Fig. 2).

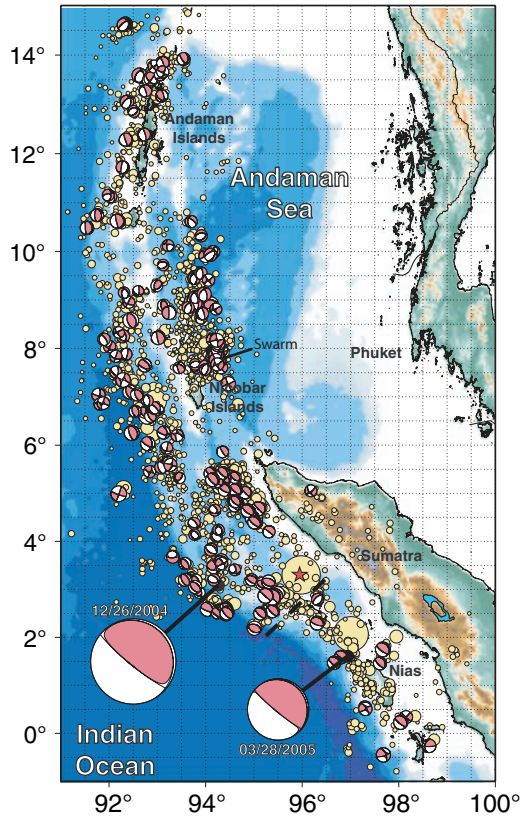

Fig. 2. Map showing aftershock locations for the first 13 weeks after the 26 December 2004 earthquake from the NEIC (yellow dots, with radii proportional to seismic magnitude). Moment-tensor solutions from the Harvard CMT catalog (*21*) are shown for the 26 December 2004 and 28 March 2005 mainshocks (large solutions at bottom, with associated centroid locations) and aftershocks. Star indicates the epicenter for the 2004 rupture obtained by the NEIC. Dashed line shows the boundary between the aftershock zones for the two events.

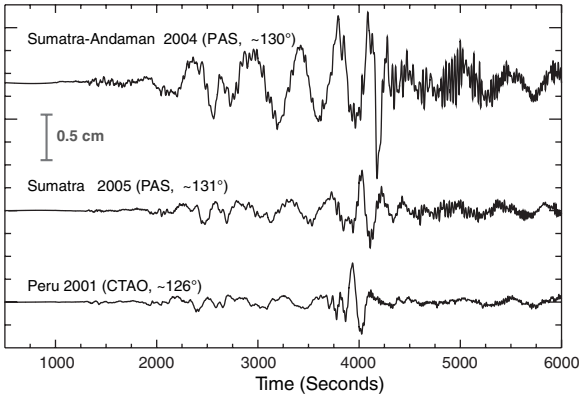

Fig. 3. Vertical-component ground displacements for periods <1000 s observed for the three largest earthquakes of the past 40 years. The upper trace shows the seismogram from the 26 December 2004 Sumatra-Andaman earthquake observed 130° away in Pasadena, California, USA; the middle trace is for the 28 March 2005 Sumatra earthquake observed 131° away in Pasadena, California, USA; the lower trace shows a seismogram for the 23 June 2001 M_w 8.4 earthquake off the coast of Peru, observed 126° away in Charters Towers, Australia. Additional waveforms are shown in fig. S4.

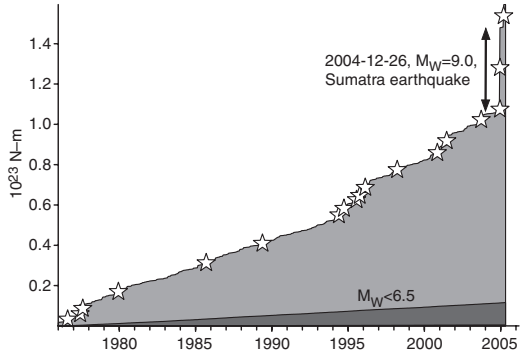

Fig. 4. Plot of cumulative seismic moment as a function of time for the 29-year history of the Harvard CMT catalog, which contains results for global earthquakes of magnitude larger than ~5.0, with great ($M_w \geq 8$) earthquakes indicated by stars. The 300- to 500-s period seismic moment for the 2004 event is comparable to the cumulative global earthquake seismic moment release for the preceding decade.

Peak-to-peak ground motions for the 2004 event exceeded 9 cm in Sri Lanka, 15.5° from the epicenter, and long-period surface-wave motions exceeded 1 cm everywhere on Earth's surface (*7*) (fig. S4). This giant event produced motions (Fig. 3) that dwarf those of the 2005 event and the 23 June 2001 Peru earthquake (M_w = 8.4), the largest earthquake previously recorded by global broadband seismometers (*22*). The high-quality global recordings enable seismological quantification of these great earthquakes (*23*).

Aftershock geometry. Harvard CMT focal mechanisms for aftershocks (Fig. 2) display a variety of geometries, including thrust faulting along the subduction zone and strike slip and normal faulting in the Andaman Sea back arc. These mechanisms are generally consistent with the expected slip partitioning along the boundary, with nearly arc-normal thrusting in the shallowly dipping subduction zone and right-lateral shearing in the back arc.

The most notable aftershock feature is a swarm of strike-slip and normal faulting events in the Andaman Sea back-arc basin (Fig. 2) involving more than 150 magnitude 5 and greater earthquakes that occurred from 27 to 30 January 2005 (*20*, *21*). Previous swarms of events have occurred in this region (e.g., July 1984), but this is the most energetic earthquake swarm ever observed globally. This swarm activity can be seen as part of the overall interplate motion partitioning.

Although aftershock mechanism variability and location uncertainty make it difficult to constrain the fault geometry in detail using

seismicity, the megathrust appears to be about 240 km wide along northwestern Sumatra, extending to a depth of about 45 km. Along the Nicobar and Andaman Islands, the megathrust fault plane appears to be no more than 160 to 170 km wide, extending to a depth of about 30 km.

Magnitude, source strength, and energy. The Harvard CMT solution for the 2004 earthquake, based on global FDSN recordings of 300- to 500-s period surface waves, has a seismic moment $M_o = 4.0 \times 10^{22}$ Nm (*24*), comparable to the cumulative seismic moment of all earthquakes for the preceding decade (Fig. 4). This moment yields $M_w = 9.0$, the widely quoted seismic magnitude for the mainshock. Uniform slip of about 5.0 m over a 1300-km-long fault varying in width from 240 to 160 km with rigidity $\mu = 3.0 \times 10^{10}$ N/m^2 would account for the CMT seismic-moment estimate. Larger slip on a smaller fault area in the south would also match the seismic moment. The CMT seismic moment for the 2005 mainshock is $M_o = 1.1 \times 10^{22}$ Nm ($M_w = 8.6$).

M_w is intended to characterize the earthquake process in terms of its final, static offset but is usually based on measurements of long-period seismic waves. For very large earthquakes, these measurements are typically made at periods of 100 to 300 s, the range of commonly observed seismic surface waves like those in Fig. 3. Magnitudes of the 1960 Chile ($M_w = 9.5$), the 1964 Alaska ($M_w = 9.2$), and the 2004 Sumatra-Andaman ($M_w = 9.0$) earthquakes were all estimated from measurements around 300 s (*25*–*27*). In this sense, their magnitudes can be directly compared. The 100- to 300-s period surface-wave amplitudes for the 1964 Alaska earthquake were about three times as large as those for the 2004 Sumatra-Andaman earthquake.

When an estimate of the seismic moment is made at periods too short to represent fully the earthquake source process, the result is an underestimate of the earthquake size. Given the high-quality seismic data available for the 2004 earthquake, the effective source strength (*28*) can be determined over a broad range of frequencies with relatively good confidence (Fig. 5). For an assumption of uniform faulting geometry, the strength of the seismic-wave excitation for periods >500 s was enhanced by a factor of 1.5 to 2.5 compared with that at 300 s (*9*, *10*). The moment magnitude of the Sumatra-Andaman earthquake may thus be larger than 9.0 by 0.1 to 0.3 units (*29*). The data for the Chile and Alaska earthquakes are insufficient to determine the magnitude at very long periods. Even at 300 s, considerable uncertainty is involved in the values of M_w for old events because of data limitations. As a result, comparison of M_w for these events to one or two tenths of a magnitude unit is not meaningful. These three earthquakes should instead be compared with respect to all aspects of their source characteristics (e.g., source spectrum, radiated energy, slip distribution, and rupture speed).

Short-period radiation is particularly important for ground accelerations and intensity of structural damage. Estimates of seismic intensity, based on relative measures of structural damage and vibration, indicate intensity IX in the vicinity of Banda Aceh, intensity VII in Port Blair in the Andaman Islands, and a relatively low intensity II to IV around the Bay of Bengal (*12*, *30*). The overprinting devastation from the tsunami complicates the estimation of high-frequency effects, but intensity IX is consistent with the short-period magnitudes $m_b = 7.0$ estimated by the USGS and $\dot{m}_b = 7.2$ reported here, the latter being about 0.3 magnitude units lower than for the 1964 Alaska earthquake (*31*, *32*) (fig. S5). These values imply that the 2004 event was not depleted in high-frequency radiation, unlike the notable 1992 Nicaragua tsunami earthquake (*33*).

The energy radiated by seismic waves, E_R, is an important macroscopic seismic parameter, because the amount of potential energy partitioned to E_R reflects the physical process of the source (*34*). Unfortunately, accurate estimation of E_R, especially for great earthquakes with long source durations, is difficult. An estimate of $E_R = 1.1 \times 10^{18}$ J is obtained for the 2004 event from P waves at 11 stations over a distance range of 45° to 95° (*35*–*37*). Energy estimates for earlier giant earthquakes are based only on magnitude-energy relationships, so meaningful comparisons are difficult. The radiated energy estimated here is about 10 times that of the

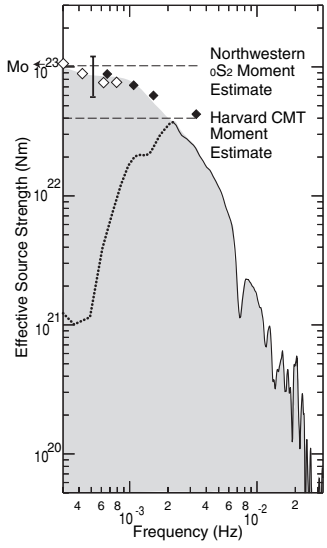

Fig. 5. Rayleigh-wave source-time function (STF) amplitude spectrum (solid and dotted line) computed by stacking more than 200 R_1 observations obtained by deconvolution of propagation effects in the frequency domain. We used a signal duration ranging from 750 to 2000 s (depending on source-receiver distance) zero-padded to 6000 s to estimate each spectrum. The dotted portion of the spectrum indicates frequencies for which the R_1 spectral amplitudes are not well resolved. White diamonds show estimates of moment from free oscillations ($_0S_2$, $_0S_3$, $_0S_4$, and $_0S_0$, from left to right) made by Northwestern University. Black diamonds show spectral levels estimated by comparison of filtered time-domain signals with synthetics for the Harvard CMT solution. Effective source strengths from the Harvard CMT solution (300 to 500 s) and that estimated from $_0S_2$, assuming the Harvard CMT faulting geometry, are indicated with dashed lines. The lowest frequency level, extrapolated to zero frequency, corresponds to the seismic moment, M_o. The approximate uncertainty for all of the low-frequency estimates is about a factor of 2. The bar indicates a corresponding range of uncertainty. The shaded region represents the composite source spectrum.

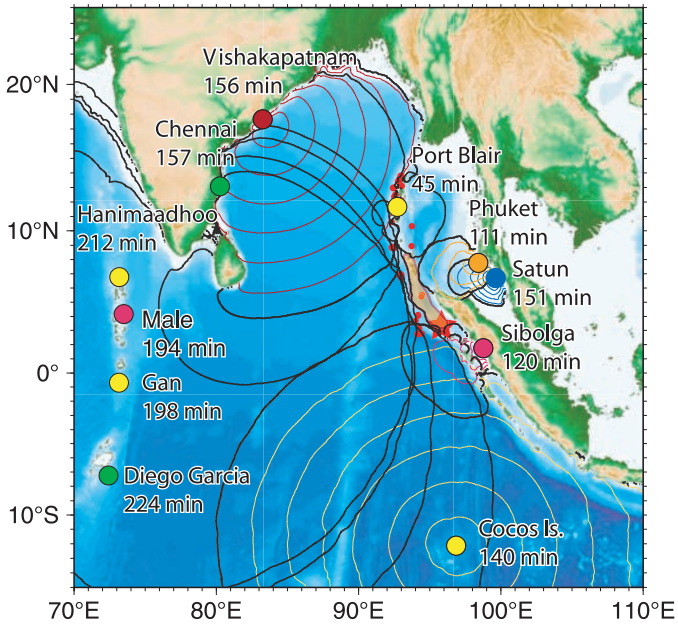

Fig. 6. Constraints on the tsunami source area obtained from the timing of tsunami arrivals at various locations around the Indian Ocean. Dark lines indicate the distance from the observing points from which tsunami might have generated at the event origin time. The tsunami source area outlined by these curves (brown region) appears to extend only 600 to 800 km north-northwest from the epicenter.

1994 deep Bolivia earthquake (M_w = 8.3) and about 40 times that of the 2001 Peru earthquake (M_w = 8.4) (Fig. 3).

Slip process of the 2004 event. The 2004 Sumatra-Andaman earthquake had the longest known earthquake rupture. Short-period seismic body waves (0.5 to 0.25 s) show azimuthally varying durations that indicate that the seismic rupture front propagated to about 1200 km north of the epicenter with a rupture velocity of about 2.0 to 3.0 km/s and that short-period radiation was generated for at least 500 s (*38*). Array analysis of 1- to 2-s period seismic waves from Hi-net stations in Japan yields compatible results (*39*). Analysis of longer period body waves and surface waves demonstrates that most of the slip that generated seismic waves was concentrated in the southern half of the rupture zone, with diminishing, increasingly oblique slip toward the north on the fault (*9*). The seismic moment of models that successfully match the long-period body- and surface-wave data is about 1.5 times as large as the CMT moment, consistent with free oscillation observations (*10*).

The seismic model does not, however, account for all observations. Geodetic constraints require two to three times more slip in the north (*40*). This suggests rupture of the northern region with a long source-process time that generated little or no seismic waves. Well-documented tilting in the Andaman and Nicobar Islands (*12*), with the western margins of the islands being uplifted and the eastern margins being submerged, can be accounted for by substantial slip of about 10 m on a 160-km-wide thrust plane in the northern half of the rupture zone or by less slip on more steeply dipping splay faults. Such large slip must have occurred on time scales longer than 1000 s, because it did not generate strong seismic-wave radiation late in the rupture.

Arrival times of tsunami waves around the Sea of Bengal provide additional constraints on the slip distribution in the north. Bounds can be placed on the location of ocean-bottom uplift due to faulting by back-propagating the initial tsunami wavefront from tsunami recording locations to the source region. The source region for strong initial tsunami excitation extends 600 to 800 km north of the epicenter, terminating near the Nicobar Islands (*41*) (Fig. 6 and fig. S6). The northern third of the aftershock zone appears not to have produced rapid vertical ocean-bottom displacements capable of generating large tsunami waves (fig. S7), but delayed slip cannot be ruled out. This estimate of the tsunami source region is consistent with satellite altimetry observations of the deep-water waves obtained by fortuitous passage of two satellites over the Indian Ocean 2 to 3 hours after the rupture occurred (*42*) (Fig. 7).

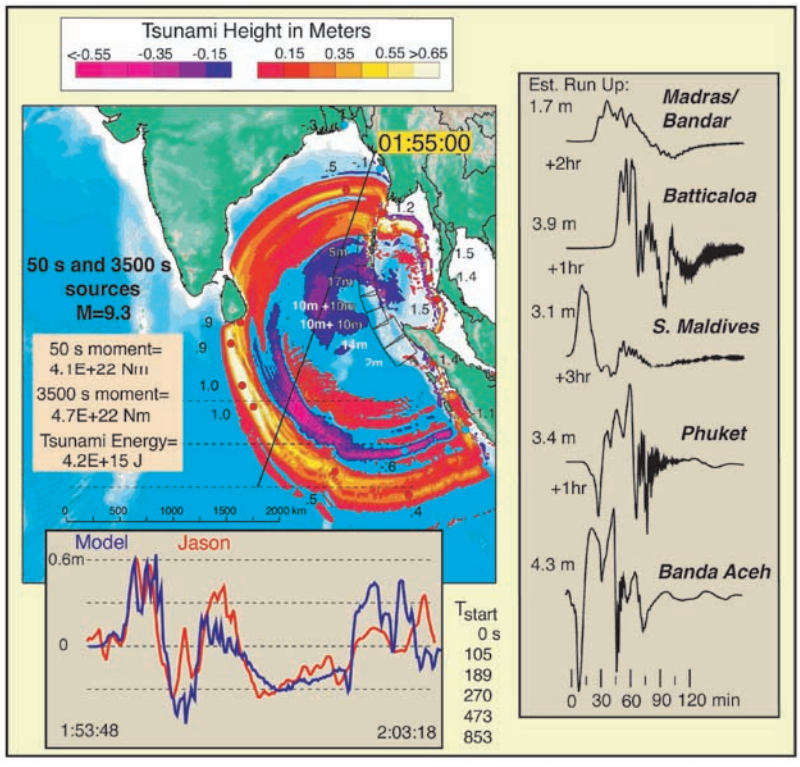

Fig. 7. **(Left)** Tsunami model at a time of 1 hour 55 min after earthquake initiation, computed for a composite slip model with fast slip (50-s rise time) in the southern portion of the rupture and slow slip (3500-s rise time) in the north. The northward propagating rupture velocity is about 2 km/s for the first 745 km, then slows to 750 m/s. The amplitude of fast and slow slip on the six fault segments are indicated by white numbers and outlined numbers, respectively. The overall seismic moment of 8.8 × 10^{22} Nm (μ = 3.0 × 10^{10} N/m^2) is divided fairly evenly between slow and fast contributions. Red colors in the map indicate positive ocean wave height, blue colors negative. The numbers along the wavefront give wave amplitudes in meters. Diagonal line is the track of the Jason satellite that passed over the region at about this time (10 min of actual transit time along the profile). The predicted (blue) and observed (red) tsunami wave are shown in the inset. The tsunami generated by the fast component of slip alone cannot explain the trough in the central Bay of Bengal (fig. S8 and Movie S1). **(Right)** Tsunami waveforms and estimated run-up heights for five locations around the Bay of Bengal. The first arrivals show water draw-down toward the east and inundation toward the west. Principal wave period is about 30 min.

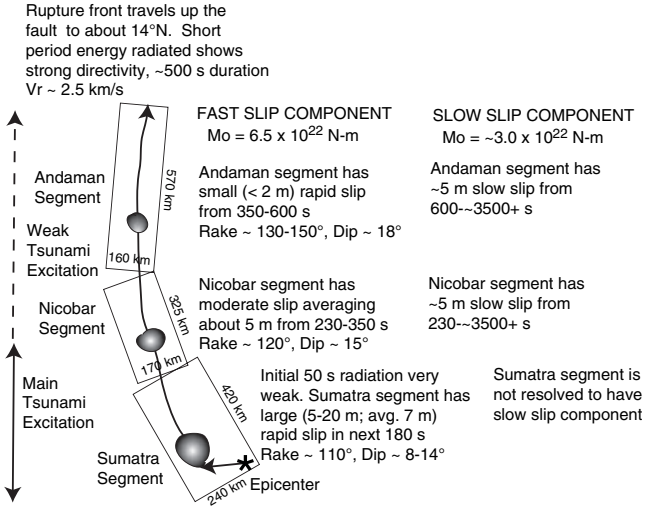

Fig. 8. Summary rupture scenario for the 2004 Sumatra-Andaman earthquake. We subdivide the rupture zone into three segments according to the inferred rupture process, not because of clear physical fault segmentation. The rupture begins at the southeastern edge of the Sumatra segment, with the initial 50 s of rupture characterized by fairly low energy release and slow rupture velocity. The rupture front then expands to the north-northwest at about 2.5 km/s, extending about 1300 km. Short-period radiation tracks the rupture front, with a total duration of about 500 s and clear north-northwest directivity. Large, rapid slip occurs in the Sumatra segment, with some patches having slip as great as 20 m during the first 230 s. The Nicobar segment has weaker slip during the next 2 min, and the Andaman segment fails with little (<2 m) rapid slip. Slow slip appears to continue in the Nicobar and Andaman segments, with a total duration of about 1 hour. The precise amount of slip and total moment of the slow-slip component are not well resolved, but about 10 m of slip under the Andaman Islands is required to account for the tilt experienced by the islands.

The tsunami calculation shown in Fig. 7, which provides a generally satisfactory fit to the satellite observations, uses a finite-fault model with the same geometry as that providing a good fit to the seismic data but with somewhat different slips, rise times, and start times on each segment (Movie S1). A broad trough in the ocean surface in the central Sea of Bengal 2 hours after the earthquake can be modeled well if slow slip occurred over ~1 hour under the Nicobar and Andaman Islands (fig. S8 shows the prediction for a model with no slow slip). This is currently the strongest constraint on the source-process time for the slow-slip component of the 2004 event. The tsunami energy computed for this composite model is 4.2×10^{15} J, less than 0.5% of the strain energy released by the faulting. Tsunami generation is not a very efficient process, but tremendous destruction can clearly result from this small component of the energy budget. No slow slip has yet been resolved for the 28 March 2005 event (*9*) (Movie S2).

Discussion. The 2004 Sumatra-Andaman earthquake rupture appears to have been a compound process of seismic-energy release, involving variable slip amplitude, rupture velocities, and slip duration. About 90 to 95% of the seismic observations can be accounted for with the rupture model (*9*, *10*) depicted schematically in Fig. 8.

The northern portion of the fault appears to have slipped 3 to 7 m more than accounted for by the seismic model, with a time scale of ~1 hour or longer. The cause of the compound slip behavior is not well-understood. It appears that the slow slip occurred only along the Nicobar and Andaman Islands segments of the rupture zone, where the plate convergence is increasingly oblique and slip is strongly partitioned. For the low convergence rate of 14 mm/year in the region, it would take 700 years to accumulate 10 m of slip potential in the region, which is consistent with the lack of historical great events in the northern part of the subduction zone.

The age of the subducting oceanic plate increases from about 60 million to 90 million years between Sumatra and the Andaman Islands, and this change may also influence mechanical coupling on the thrust plane. Subduction of younger lithosphere tends to result in interplate faults with shallow dips and broad contact areas that generate great earthquakes, whereas in locations where older lithosphere is subducted and back-arc spreading is observed, great earthquakes are rare (*43*–*45*). The strong lateral gradient in obliquity of interplate motion and the rapid increase in age of the subducting oceanic plate toward the north-northwest are distinctive features compared with the settings of previous great earthquakes. The most analogous tectonic environment may be the western Aleutians, where the 1965 (M_w = 8.7) Rat Island earthquake occurred along a curving plate boundary with increasing obliquity of interplate motion along the arc (*46*).

Logical regions for concern about future large earthquakes are along the Sumatra Fault and southeast of the 2005 event rupture; the adjacent region failed in 1833 and is likely to have accumulated substantial strain. International efforts to improve tsunami-warning capabilities in the Indian Ocean are warranted given the inevitability of future great thrust earthquakes along the Sumatra subduction zone.

References and Notes

1. The February 23, 2005 update on the U.S. Geological Survey (USGS) Web site http://earthquake.usgs.gov/eqinthenews/2004/usslav indicates 283,100 confirmed fatalities, 14,100 missing, and 1,126,900 displaced. The majority of the fatalities were in Indonesia (235,800), with 30,900 fatalities in Sri Lanka.
2. K. Abe, personal communication, 2005.
3. K. Abe, *J. Geophys. Res.* **84**, 1561 (1979).
4. http://earthquake.usgs.gov/eqinthenews/2005/usweax indicates more than 1300 fatalities on Nias, Simeulue, Kepulauen Banyak, and Meulaboh.
5. R. Butler *et al.*, *EOS Trans. Am. Geophys. Union* **85**, 225 (2004); http://www.iris.edu.
6. B. A. Romanowicz, D. Giardini, *Science* **293**, 2000 (2001).
7. J. Park *et al.*, *EOS Trans. Am. Geophys. Union* **86**, 57 (2005).
8. J. Park *et al.*, *Seismol. Res. Lett.*, in press (2005).
9. C. J. Ammon *et al.*, *Science* **308**, 1133 (2005).
10. J. Park *et al.*, *Science* **308**, 1139 (2005).
11. K. R. Newcomb, W. R. McCann, *J. Geophys. Res.* **92**, 421 (1987).
12. R. Bilham, E. R. Engdahl, N. Feldl, S. P. Satyabala Seism., *Seismol. Res. Lett.*, in press (2005).
13. Y. Bock *et al.*, *J. Geophys. Res.* **108**, 2367 (2003).
14. J. Paul *et al.*, *Geophys. Res. Lett.* **28**, 657 (2001).
15. R. McCaffrey, *J. Geophys. Res.* **97**, 8905 (1992).
16. K. Sieh, D. Natawidjaja, *J. Geophys. Res.* **105**, 28295 (2000).
17. J. Zachariasen *et al.*, *J. Geophys. Res.* **104**, 895 (1999).
18. D. H. Natawidjaja *et al.*, *J. Geophys. Res.* **109**, B04306, doi:10.1029/2003JB002398 (2004).
19. W. R. McCann, S. P. Nishenko, L. R. Sykes, J. Krause, *Pure Appl. Geophys.* **117**, 1082 (1979).
20. G. Ekström, A. M. Dziewonski, N. N. Maternovskaya, M. Nettles, *Phys. Earth Planet Inter.* **148**, 327 (2005).
21. Harvard CMT solutions can be accessed at http://www.seismology.harvard.edu/CMTsearch.html.
22. M. K. Giovanni, S. L. Beck, L. Wagner, *Geophys. Res. Lett.* **29**, 2018, doi:10.1029/2002GL015774 (2002).
23. Many stations of the Global Seismographic Network operated by the Incorporated Research Institutions for Seismology, the University of California, San Diego, and the USGS are connected by real-time telemetry to operational efforts of the USGS National Earthquake Information Center and the National Oceanic and Atmospheric Administration Pacific Tsunami Warning Center. These centers provide rapid earthquake location, seismic-magnitude, and tsunami-potential determinations (*8*).
24. Seismic moment is a measure of overall earthquake size, equal to the product of the rigidity of the material around the rupture zone, μ, the total fault area, A, and the average displacement across the fault, D ($M_o = \mu AD$).
25. For the Alaska and Chile events, the amplitude measurements are made at 300 s, but the zero-frequency seismic-moment value is estimated using a finite-source model.
26. H. Kanamori, *J. Geophys. Res.* **75**, 5029 (1970).
27. H. Kanamori, J. J. Cipar, *Phys. Earth Planet. Inter.* **9**, 128 (1974).
28. The amplitude spectrum in Fig. 5 is constructed as follows. The CMT solution has a specific moment-rate spectrum, $M_0^{CMT}(f)$, as a function of frequency, used to predict the displacement spectrum, $S_0^{CMT}(f)$, at a particular position. Let the observed spectrum at that position determined from normal modes or long-period surface waves be $S_0^{obs}(f)$. We define the relative moment-rate spectrum, $M_0^{obs}(f)$, by $M_0^{obs}(f) = \left(\frac{S_0^{obs}(f)}{S_0^{CMT}(f)}\right) M_0^{CMT}(f)$, yielding the effective source strength shown in Fig. 5. $M_0^{obs}(f)$ depends on $S_0^{CMT}(f)$, which in turn depends on the CMT source mechanism and depth and the modeling assumptions in the CMT solution.
29. If the dip angle increases toward the north, the moment determined here will be overestimated. A change in dip from 8° to 12° would reduce the estimated moment by 50%, and if the dip were 15° or more in the subduction zone along the Andaman Islands, the effect could be even larger. The increase in low-frequency source strength seen in Fig. 5 could thus be an artifact of using too shallow a dip for the northern portion of the rupture.
30. See http://pasadena.wr.usgs.gov/shake/ous/STORE/Xslav_04/ciim_display.html.
31. The standard seismic body-wave magnitude, m_b, involves the peak ground motion near a period of 1 s in the first few cycles of the *P* wave. For great earthquakes, the short-period energy usually continues to grow for some time, and a modified magnitude, $\hat{m}_b$, was introduced (*32*) to use the maximum ground motion of the short-period *P*-wave arrival. For events larger than $M_w = 6.5$, an empirical relation of $\hat{m}_b = 0.53\, M_w + 2.70$ has been observed. Comparisons of $\hat{m}_b$ with seismic moment are shown for many large earthquakes, including the Sumatra-Andaman event, in fig. S5.
32. H. Houston, H. Kanamori, *Bull. Seismol. Soc. Am.* **76**, 19 (1986).
33. H. Kanamori, M. Kikuchi, *Nature* **361**, 714 (1993).
34. H. Kanamori, *Proc. Jpn. Acad. Ser. B* **80**, 297 (2004).
35. E_R is estimated by the method of (*36*), using *P*-wave trains with a duration of 400 s. The contribution from later phases like *PP* and *PPP* is empirically estimated using the records of the 26 January 2001 India earthquake. For that event, the source duration is known to be shorter than 50 s. Thus, the ratio of E_R (1.4) estimated from the 400-s and 50-s records of the India earthquake represents the contribution of the later phases, and this ratio can be used to correct for the contribution of the later phases for the Sumatra-Andaman earthquake. The value of E_R, thus estimated, is 10 times as large as that listed by the USGS (*1*) (http://neic.usgs.gov/neis/eq_depot/2004/eq_041226/neic_slav_e.html). This difference is probably due to the difference in the durations of the records used for estimation. An estimate of E_R for the event can also be made based on the CMT seismic moment and conventional assumptions about the stress drop and the stress-release mechanism (*37*), which gives $E_R = 2 \times 10^{18}$ J (475 megatons energy equivalent), but this great rupture may not satisfy conventional assumptions. The 20-s-period surface-wave magnitude is $M_S = 8.8$, a measure that is expected to be low relative to magnitude measures at longer periods because of the long source duration relative to 20 s. Using this value in the Gutenberg M_S-E_R relationship gives $E_R = 1.0 \times 10^{18}$ J.
36. A. Venkataraman, H. Kanamori, *J. Geophys. Res.* **109**, B05302, doi:10.1029/2003JB002549 (2004).
37. H. Kanamori, *J. Geophys. Res.* **82**, 2981 (1977).
38. S. Ni, H. Kanamori, D. Helmberger, *Nature* **434**, 582 (2005).
39. M. Ishii, P. Shearer, H. Houston, J. Vidale, *Nature*, in press (2005).
40. P. Banerjee, F. F. Pollitz, R. Bürgmann, *Science* 19 May 2005 (10.1126/science.1113746).
41. The tsunami source region estimated in Fig. 6 and shown in greater detail in fig. S6 is based on back-projecting tsunami waves from arrival points with known arrival times to the origin time of the earthquake. This provides a lower bound of 600-km length

for the tsunami source area, based on assumptions of instantaneous rupture and total slip on the fault. If we allow for the delay in tsunami excitation due to finite rupture propagation time to the Nicobar region (~3 to 4 min), along with delay in excitation due to finite-slip rise time (1 to 5 min), the effective tsunami source area may extend to 10°N, giving a total source region about 800 km long.
42. J. Gower, *EOS Trans. Am. Geophys. Union* **86**, 37 (2005).
43. S. Uyeda, H. Kanamori, *J. Geophys. Res.* **84**, 1049 (1979).
44. L. Ruff, H. Kanamori, *Tectonophysics* **99**, 99 (1983).
45. R. Scholz, J. Campos, *J. Geophys. Res.* **100**, 22,103 (1995).
46. F. T. Wu, H. Kanamori, *J. Geophys. Res.* **78**, 6082 (1973).
47. This work was supported in part by the U.S. National Science Foundation under grants EAR-0125595, EAR-0337495, and EAR-0207608. Seismic waveform data from the Global Seismographic Network (funded by NSF under Cooperative Agreement EAR-0004370 and USGS) were obtained from the Incorporated Research Institutions for Seismology (IRIS) Data Management System. Jason data were provided by Lee-Lueng Fu of the Jet Propulsion Laboratory in Pasadena, CA.

Supporting Online Material
www.sciencemag.org/cgi/content/full/308/5725/1127/DC1
Figs. S1 to S8
Table S1
Movies S1 and S2

14 March 2005; accepted 25 April 2005
10.1126/science.1112250

RESEARCH ARTICLE

Rupture Process of the 2004 Sumatra-Andaman Earthquake

Charles J. Ammon,[1]* Chen Ji,[2] Hong-Kie Thio,[3] David Robinson,[4] Sidao Ni,[5,2] Vala Hjorleifsdottir,[2] Hiroo Kanamori,[2] Thorne Lay,[6] Shamita Das,[4] Don Helmberger,[2] Gene Ichinose,[3] Jascha Polet,[7] David Wald[8]

The 26 December 2004 Sumatra-Andaman earthquake initiated slowly, with small slip and a slow rupture speed for the first 40 to 60 seconds. Then the rupture expanded at a speed of about 2.5 kilometers per second toward the north northwest, extending 1200 to 1300 kilometers along the Andaman trough. Peak displacements reached ~15 meters along a 600-kilometer segment of the plate boundary offshore of northwestern Sumatra and the southern Nicobar islands. Slip was less in the northern 400 to 500 kilometers of the aftershock zone, and at least some slip in that region may have occurred on a time scale beyond the seismic band.

Seismic waves are excited by rapid and varying sliding motions that initiate with a frictional instability. Slip begins as the rupture front spreads across the fault with a velocity usually less than the ambient shear wave speed. Both rupture propagation and local slip history (the temporal variation and total slip at a particular position on a fault) influence the frequency and strength of radiated seismic waves. Different positions on the fault generally have different displacement histories, including variations in the rate and amount of slip. Seismic waves sense these differences, and by using ground motions observed far from the source seismologists can reconstruct the spatial and temporal slip history of faulting.

Several phenomena affect seismic wave excitation during faulting. One is the stress drop at the rupture front. As the rupture front expands, short-period P and S waves are generated from the local stress reduction. For large events, these waves can be used to map the earthquake's rupture expansion. The speed of rupture front propagation, which can be related to the energy partitioning during the faulting process, is an important quantity. The potential energy released during earthquakes is partitioned into seismic radiation, mechanical processes such as creation of fractures, and frictional heat (*1*). The amount of heat generated by frictional processes during the rupture depends on the absolute stress, total slip, and rupture area. The partitioning of energy between mechanical processes and seismic radiation varies from earthquake to earthquake and provides one method of classifying different faulting processes. Fast ruptures can be associated with a relatively large fraction of seismically radiated energy (*1*, *2*). For many well-studied earthquakes, the rupture speed is 70 to 95% of the shear wave velocity, but important variations have been observed as complex ruptures cross fault-segment boundaries (*3*). Another important observation is the spatial pattern of slip in large earthquakes. For many shallow earthquakes, slip near the hypocenter is relatively small, indicating to some extent that the earthquake began at a weak region and grew into a much larger event (*1*). These observations are extracted from analysis of the seismic wave field. The 26 December 2004 Sumatra-Andaman and the 28 March 2005 earthquakes (*4*) produced the most extensive high-quality broadband seismic data ever recorded for great earthquakes. Here, we exploit signals across a broad bandwidth and every part of the seismic wave field to construct an integrated seismic view of these earthquake ruptures. Our focus is on the first and larger of the two events.

Short-period *P*-wave directivity. Short-period P-wave radiation (*5*) for large earthquakes provides direct information about the rupture front propagation. The energy radiated by an expanding rupture front can be observed with the use of the global seismic networks (*6*) or regional seismic and hydroacoustic arrays (*7*–*9*). One of the simplest measures that can be made is the duration of short-period P-wave radiation from the source region (*10*, *11*). For a long-duration earthquake, a major challenge for P-wave analysis is the interference of later-arriving seismic waves reflected from the surface and discontinuities in the Earth with P waves radiated from later portions of the rupture. Fortunately, most secondary phases involve additional path segments in the highly attenuating upper mantle, and their short-period content is suppressed (*12*). Applying a high-pass filter can reduce the effects of secondary arrivals. The durations of short-period P waves will be shorter in the direction of rupture propagation and longer in the direction away from the moving source (the rupture front). Data for the Sumatra-Andaman earthquake (Fig. 1) indicate a north-northwest rupture propagation with a speed of about 2.5 km/s and an overall fault length of 1200 to 1300 km, a length consistent with the aftershock distribution (*4*).

The amplitude of the short-period waveforms generated during the rupture also varied about a relatively uniform level. At least three large (from 50 to 150 s, 280 to 340 s, and 450 to 500 s) and several additional seismic

[1]Department of Geosciences, Pennsylvania State University, 440 Deike Building, University Park, PA 16802, USA. [2]Seismological Laboratory, California Institute of Technology, MS 252-21, Pasadena, CA 91125, USA. [3]URS Corporation, 566 El Dorado Street, Pasadena, CA 91101, USA. [4]Department of Earth Sciences, University of Oxford, Parks Road, Oxford OX1 3PR, UK. [5]Chinese Academy of Sciences Key Laboratory of Crust-Mantle Materials and Environments, University of Science and Technology of China, Hefei, Anhui 230026, China. [6]Earth Sciences Department and Institute of Geophysics and Planetary Physics, University of California, Santa Cruz, CA 95064, USA. [7]Institute for Crustal Studies, Santa Barbara, CA 93106, USA. [8]National Earthquake Information Center, U.S. Geological Survey (USGS), Golden, CO 80401, USA.

*To whom correspondence should be addressed. E-mail: cammon@geosc.psu.edu